Dielectric function of the Si(113)3×2ADI surface from ab-initio methods

Katalin Gaál-Nagy* and Giovanni Onida

*Dipartimento di Fisica and ETSF, Università degli Studi di Milano, via Celoria 16, I-20133 Milano, Italy *E-mail: katalin.gaal-nagy@physik.uni-regensburg.de*

We have investigated the imaginary part of the dielectric function Im(ϵ) of the (113) 3×2 ADI reconstructed surface of silicon. The calculations have been performed for a periodic slab within the plane-wave pseudopotential approach to the density-functional theory. The three diagonal components of Im(ϵ) have been derived from the momentum matrix elements within the independent particle random phase approximation (IPRPA). In this article, the importance of the **k**-point convergence is figured out by inspecting **k**-point resolved spectra.

Keywords: ab initio calculations, optical properties, high-index silicon surfaces

1. Introduction

The Si(113) surface is one of the most stable high-index surfaces of Si [1]. It is used as a substrate for the self-assembled growth of Ge nanowires and Ge as well as SiGe islands[2–5]. Since this surface is atomically smooth, ultrathin oxide films can be grown on Si(113)[6,7], which is hence also dealt as a candidate for wafers and devices.

The clean surface shows a 3×2 periodicity at room temperature which can transform into a 3×1 one by a phase transition induced by high temperatures or contamination[8,9]. The most probable is the Si(113)3×2ADI (adatom-dimer-interstitial) reconstruction, which was proposed by Dąbrowski et al.[10] (see Fig. 1). Comparing ab-initio results for reasonable surface models, the ADI reconstruction has the lowest surface energy[11]. Besides, an experimental confirmation is given by STM measurements[4,12]. However, still other models can not be ruled out[13].

A complementary study of the Si(113)3×2 surface can be done by the investigation of its optical properties, e.g., the reflectance anisotropy spectra (RAS). At the aim of performing a theoretical ab-initio investigation of the optical properties the first step is the calculation of the imaginary part of

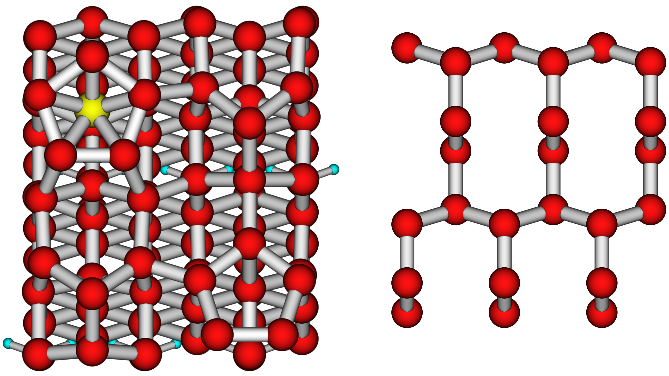

Fig. 1. In the left panel, a top view (x-y plane) of the Si(113)3×2ADI reconstruction is shown. The right panel displays a top view of just two "double layers" of the bulk-like part of the slab. The Si atoms are dark (the interstitial Si atom light) and the hydrogen atoms light.

the dielectric function Im(ϵ). Results for Im(ϵ) are presented in this work.

2. Method

The calculations have been performed within the plane-wave (PW) pseudopotential approach to the density-functional theory[14,15] as implemented in ABINIT[16] and TOSCA[17]. For the exchange-correlation energy the local-density approximation has been used[18,19]. The ground state convergence required 4 **k** Monkhorst-Pack[20] points in the irreducible wedge of the Brillouin zone (IBZ) as well as a kinetic-energy cutoff of 12 Ry ($\approx$ 24000 PW). The slab used for the calculation contains 11 double layers (DL) of Si where the bottom surface is saturated with hydrogen atoms (see Figs. 1 and 4). The topmost 4 DL have been relaxed, and the remaining have been kept to bulk positions.

The imaginary part of the dielectric function Im[$\epsilon(\omega)$] as a function of the energy ω has been derived by a summation of the matrixelements of the momentum operator[21]. The sum has to be taken over the valence- and the conduction states (here: 175 and 185, respectively), and weighted **k** points, which in the present case can be taken just in one quarter of the Brillouin Zone, which is the IBZ of the system. For the layer-by-layer analysis modified matrixelements have been used according to the prescriptions of reference 22 (see also references 23 and 24). Here, the effects of local fields, self energy, and excitons have been neglected.

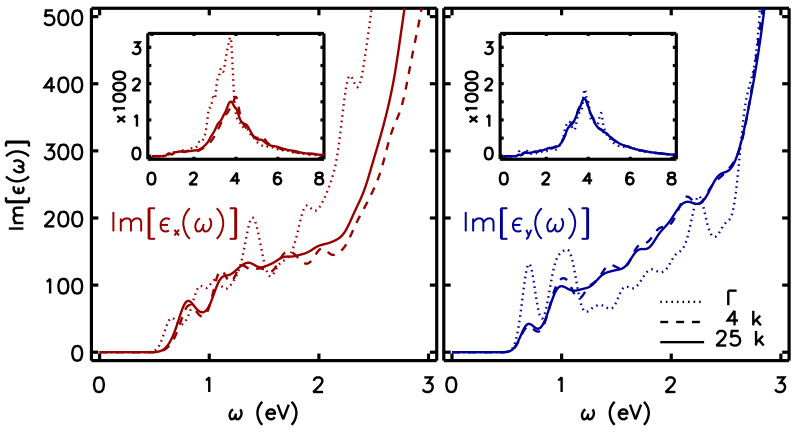

Fig. 2. $\mathrm{Im}[\epsilon_x(\omega)]$ (left) and $\mathrm{Im}[\epsilon_y(\omega)]$ (right) for various numbers of **k** points (assignment in the graph) for the low-energy range, where the surface states are found. The full energy range is shown in the insets.

3. k point convergence

For the calculation of $\mathrm{Im}[\epsilon(\omega)]$ (and consequently, for the calculation of all optical properties which are based on this) the convergence with respect to number of **k** points in the summation described above is essential, since the spectra are particularly sensitive to that. Working out of convergence can yield wrong difference spectra (e.g., RAS). In comparison, the convergence with respect to the number of bands is less demanding in the surface-related low-energy range. Thus, we performed a very careful check of the **k**-point convergence.

Since the slab was chosen with the surface perpendicular to z, $\mathrm{Im}[\epsilon(\omega)]$ should be investigated for light polarized in x and y direction, since these functions are the ingredients for difference spectra like the RAS. We show in Fig. 2 the $\mathrm{Im}[\epsilon_x(\omega)]$ and $\mathrm{Im}[\epsilon_y(\omega)]$ for various sets of **k** points. For both polarizations, at least 25 **k**-points are required. The convergence for $\mathrm{Im}[\epsilon_y(\omega)]$ is faster than for $\mathrm{Im}[\epsilon_x(\omega)]$. In particular, the differences between 4 and 25 **k** points for the $\mathrm{Im}[\epsilon_x(\omega)]$ is still significant.

In order to improve the **k**-points grid in the most efficient way, we have performed a single-**k** analysis. This means, we have inspected the contributions of each **k** point to the spectra separately, which are shown in Fig. 3. It is apparent that the changes for the $\mathrm{Im}[\epsilon_x(\omega)]$ from one **k** to a neighbouring one, especially in x direction, are larger than for $\mathrm{Im}[\epsilon_y(\omega)]$. Thus, we have chosen 30 additional **k** points in between along the x direction. The spectra

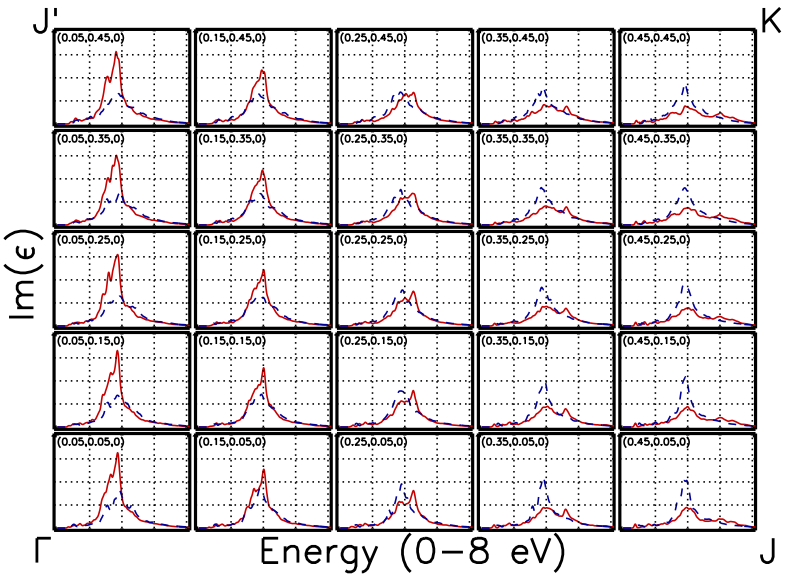

Fig. 3. Single-**k** decomposition of the spectra using 25 **k** in the surface IBZ. Im$[\epsilon_x(\omega)]$ is drawn with solid and Im$[\epsilon_y(\omega)]$ with dashed lines. The coordinates of the **k** points are denoted in the inset. The spectra are organized as the **k** points in the surface IBZ, where the Γ point is close to the low-left corner of the figure.

based on the resulting 55 **k** points (not shown in Fig. 2) demonstrates, that convergence already had been achieved with 25 **k** points. This strategy allows one to avoid a "blind" increase of the **k**-point grid, which can be very time-consuming.

4. Anisotropy at Γ

In Fig. 2 a particular feature is visible: in the contribution coming from the Γ point, a strong anisotropy at the medium-high energy range, between the x and the y polarization, occurs. This anisotropy at Γ appears in the energy range of bulk-bulk transitions. In fact, performing a layer-by-layer analysis the spatial localization of such anisotropic contributions is clearly found to be in the bulk (internal) DLs, as shown in Fig. 4, together with a side view of the slab cell where the DLs used for each spectra are marked. We have chosen always pairs of DLs, e.g., L07L08 corresponds to the spectra with contributions from DL 7 and DL 8, where the DLs are counted from the top to the bottom. Of course, bulk silicon is isotropic, which results also from calculations using a sufficient amount of **k** points. The bulk anisotropy at

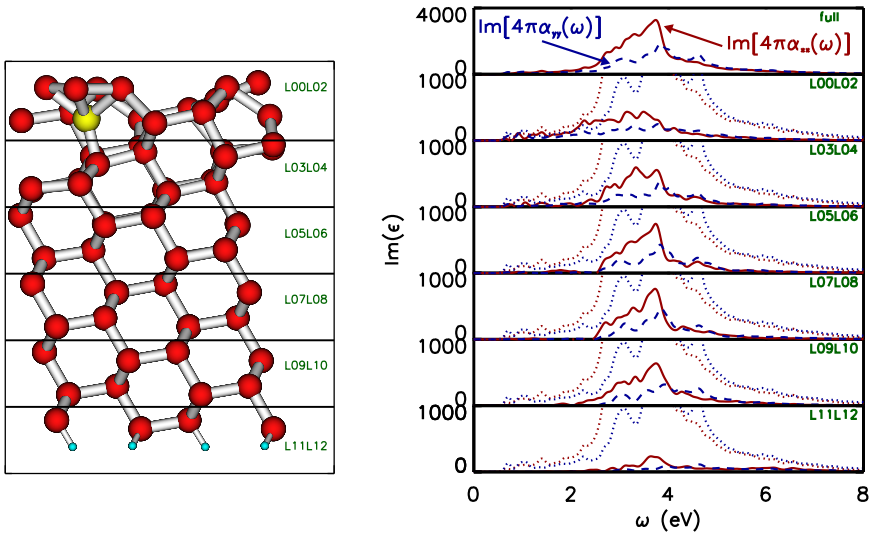

Fig. 4. Layer-by-layer decomposition of the spectra and complete spectra containing all layers (full) for the Γ point calculation (right). The spectra correspond to the layers denoted in the inset and marked at the structure (left). $\mathrm{Im}[\epsilon_x(\omega)]$ is drawn with solid and $\mathrm{Im}[\epsilon_y(\omega)]$ with dashed lines. In addition, the full-slab spectra are drawn with dotted lines. DL L00 corresponds to the vacuum at the top of the slab and DL12 to the hydrogen at the bottom.

the Γ point here is just due to the use of a low-symmetry supercell.

Fig. 4 shows that this anisotropy is present at each pair of DLs in the bulk region of the slab, where the spectra for bulk region, i.e. L09L10, L07L08, and L05L06, are nearly the same. The explanation can be found by inspecting the geometry of one pair of DLs only, which is shown on the right in Fig. 1. An highly anisotropic "chain structure" oriented along the x axis can be seen. This is the reason for the strong signal appearing at Γ (the wavefunctions are in phase and the wavelength of light is much larger than the cell dimension).

5. Summary

In summary, we have presented ab-initio results for the imaginary part of the dielectric function for the Si(113)3×2ADI surface. At this example we have shown the possibility of accelerating the convergence tests with respect to **k** points by performing a single-**k** analysis. We have applied a layer-by-layer analysis allowing us to explain a strong anisotropic contribution coming from the Γ point. The results described here are useful for further

calculations, e.g., the RAS spectra, which can be obtained from $\mathrm{Im}[\epsilon(\omega)]$.

6. Acknowledgment

This work was funded by the EU's 6th Framework Programme through the NANOQUANTA Network of Excellence (NMP4-CT-2004-500198). K.G.-N. also likes to acknowledge S. Hinrich and A. Stekolnikov for support.

References

1. D. J. Eaglesham, A. E. White, L. C. Feldman, N. Moriya and D. C. Jacobson, *Phys. Rev. Lett.* **70**, p. 1643 (1993).
2. H. Omi and T. Ogino, *Phys. Rev. B* **59**, p. 7521 (1999).
3. M. P. Halsall, H. Omi and T. Ogino, *Appl. Phys. Lett.* **81**, p. 2448 (2002).
4. Z. Zhang, K. Sumitomo, H. Omi, T. Ogino and X. Zhu, *Surf. Interface Anal.* **36**, p. 114 (2004).
5. M. Hanke, T. Boeck, A.-K. Gerlitzke, F. Syrowatka and F. Heyroth, *Appl. Phys. Lett.* **86**, p. 223109 (2005).
6. H.-J. Müssig, J. Dąbrowski and S. Hinrich, *Solid-State Electron.* **45**, p. 1219 (2001).
7. H.-J. Müssig, J. Dąbrowski, K.-E. Ehwald, P. Gaworzewski, A. Huber and U. Lambert, *Microelectron. Eng.* **56**, p. 195 (2001).
8. C. C. Hwang, H. S. Kim, Y. K. Kim, K. W. Ihm, C. Y. Park, K. S. An, K. J. Kim, T.-H. Kang and B. Kim, *Phys. Rev. B* **64**, p. 045305 (2001).
9. K. Jacobi and U. Myler, *Surf. Sci.* **284**, p. 223 (1993).
10. J. Dąbrowski, H.-J. Müssig and G. Wolff, *Phys. Rev. Lett.* **73**, p. 1660 (1994).
11. A. A. Stekolnikov, J. Furthmüller and F. Bechstedt, *Phys. Rev. B* **67**, p. 195332 (2003).
12. J. Knall, J. B. Pethica, J. D. Todd and J. H. Wilson, *Phys. Rev. Lett.* **66**, p. 1733 (1991).
13. K. S. Kim, J. U. Choi, Y. J. Cho and H. J. Kang, *Surf. Interface Anal.* **35**, p. 82 (2003).
14. P. Hohenberg and W. Kohn, *Phys. Rev.* **136 B**, p. 864 (1964).
15. W. Kohn and L. J. Sham, *Phys. Rev.* **140 A**, p. 1133 (1965).
16. `http://www.abinit.org`.
17. `http://users.unimi.it/etsf`.
18. J. P. Perdew and A. Zunger, *Phys. Rev. B* **23**, p. 5048 (1981).
19. D. M. Ceperley and B. J. Alder, *Phys. Rev. Lett.* **45**, p. 566 (1980).
20. H. J. Monkhorst and J. D. Pack, *Phys. Rev. B* **13**, p. 5188 (1976).
21. R. DelSole, Reflectance spectroscopy - theory, in *Photonic Probes of Surfaces*, ed. P. Halevi (Elsevier, Amsterdam, 1995).
22. C. Hogan, R. DelSole and G. Onida, *Phys. Rev. B* **68**, p. 035405 (2003).
23. C. Castillo, B. S. Mendoza, W. G. Schmidt, P. H. Hahn and F. Bechstedt, *Phys. Rev. B* **68**, p. R041310 (2003).
24. P. Monachesi, M. Palummo, R. DelSole, A. Grechnev and O. Eriksson, *Phys. Rev. B* **68**, p. 035426 (2003).